JOURNAL OF MATERIALS SCIENCE: MATERIALS IN MEDICINE **16** (2005) 663–669

An experimental and finite element poroelastic creep response analysis of an intervertebral hydrogel disc model in axial compression

P. SILVA[1,2,*], S. CROZIER[3], M. VEIDT[1], M. J. PEARCY[4]
[1]*Department of Mechanical Engineering, University of Queensland, Brisbane, Australia*
E-mail: Puji.silva@cmr.uq.edu.au
[2]*Centre for Magnetic Resonance University of Queensland, Brisbane, Australia*
[3]*School of Electrical Engineering and Information Technology, University of Queensland, Brisbane, Australia*
[4]*School of Mechanical, Manufacturing and Medical Engineering, Queensland University of Technology, Brisbane, Australia*

A hydrogel intervertebral disc (IVD) model consisting of an inner nucleus core and an outer anulus ring was manufactured from 30 and 35% by weight Poly(vinyl alcohol) hydrogel (PVA-H) concentrations and subjected to axial compression in between saturated porous endplates at 200 N for 11 h, 30 min. Repeat experiments ($n = 4$) on different samples ($N = 2$) show good reproducibility of fluid loss and axial deformation. An axisymmetric nonlinear poroelastic finite element model with variable permeability was developed using commercial finite element software to compare axial deformation and predicted fluid loss with experimental data. The FE predictions indicate differential fluid loss similar to that of biological IVDs, with the nucleus losing more water than the anulus, and there is overall good agreement between experimental and finite element predicted fluid loss. The stress distribution pattern indicates important similarities with the biological IVD that includes stress transference from the nucleus to the anulus upon sustained loading and renders it suitable as a model that can be used in future studies to better understand the role of fluid and stress in biological IVDs.
© *2005 Springer Science + Business Media, Inc.*

1. Introduction

The intervertebral disc (IVD) is a complex load bearing structure that is subjected to an equally complex regime of static and dynamic loads. The IVD responds to an applied load by exuding fluid both from the nucleus and the anulus primarily through the endplates [1]. A study of the IVD mechanics should involve the study of its water content, since a healthy IVD supports axial loading mainly via a pressurised nucleus pulposus. During compression, the physical pressure in the disc can exceed the nuclear swelling pressure, resulting in water loss [2, 3]. The hydration of the IVD is known to decrease with age and in degenerative states [4]. Hence the load dependant changes in disc water content resulting from loading is an important measure of disc quality and a key indicator of the stress distribution within the disc.

Hydrogels are hydrophilic polymer networks that may absorb up to thousands of times their dry weight of water [5, 6]. Since the land mark paper by Wichterle and Lim in 1960 [7] the interest in hydrogels for biomedical purposes has grown and for over 35 years hydrogels have been considered in biomedical and pharmaceutical applications due to their high water content, similarity to natural tissue and biocompatibility [8]. In particular, hydrogels have been used as possible intervertebral disc replacements, due to their ability to facilitate both the biomechanical and the physiological role that is found in the disc [8–10]. Experimental and finite element modelling of hydrogel deformations have considered their incompressible [11] poroelastic [4, 12, 13] and swelling characteristics [12, 14]. However to date there has been no study that has focussed on the changes in fluid flow characteristics in hydrogels under deformation, to investigate the effect of long term compressive loading on the stress distribution. Studying the fluid flow-stress distribution pattern for a given hydrogel system of known material properties will enable comparisons to be made between known behaviour patterns in biological IVD's that will lead to a better understanding of the interrelationship between fluid flow and stress distribution patterns in biological IVDs.

*Author to whom all correspondence should be addressed.

This paper investigates the following: (1) the design and manufacture of a hydrogel intervertebral disc physical model that mimics the long term creep response of the biological IVD including fluid loss. (2) the development of a finite element model of the hydrogel IVD that is able to (a) predict both the short term and long term deformation characteristics and (b) accurately predict the time dependant fluid loss from the disc.

2. Sample manufacturing

Poly (viny alcohol) (PVA) is among the most commonly used hydrogels for bio-medical applications. PVA is known to be biocompatible, biodegradable and heat resistant [15]. Currently PVA is being used in the research and development of artificial cartilage [16, 17]. Promising results have been shown in using PVA hydrogels as articular cartilage replacements in rabbits [16]. The use of hydrogels as intervertebral disc implant material has made a significant impact in extending the use of such implants beyond mechanical function to include physiological functions [10]. Since the Intervertebral disc is in many ways similar in function to articular cartilage, PVA was chosen as the desired material for the synthesis of the bi-component hydrogel disc.

A PVA (KURARAY POVAL PVA117) bi-component hydrogel model was manufactured (Fig. 1) consisting of a 30% by weight PVA inner disc representing the nucleus and a 35% by weight PVA outer stiffer ring representing the anulus. PVA was dissolved in a 1:1 mixture of water and Dimethyl Sulfoxide (DMSO) by weight at 120 °C for 2 h. The 35% PVA solution was injected into a cylindrical shaped mould and frozen at –10 °C for 24 h to form the annular ring. Freezing polymerises the PVA through physical cross-linking [18]. The 30% PVA solution was then injected to completely fill up the space in the annular ring, to form the nucleus. The hydrogel disc was swollen to equilibrium (with the nucleus absorbing a higher water percentage than the anulus) before any compression testing was carried out. The manufacturing technique ensured that there was no physical barrier for water diffusion between the two regions under an applied pressure gradient. This was confirmed through MR images of the hydrogel disc [19]. An analysis of the water content in each material based on equilibrium swelling weight data indicated that both materials consisted of an absolute water content in excess of 80% and that the % of "free water" (i.e. available for exudation) was in excess of 60%.

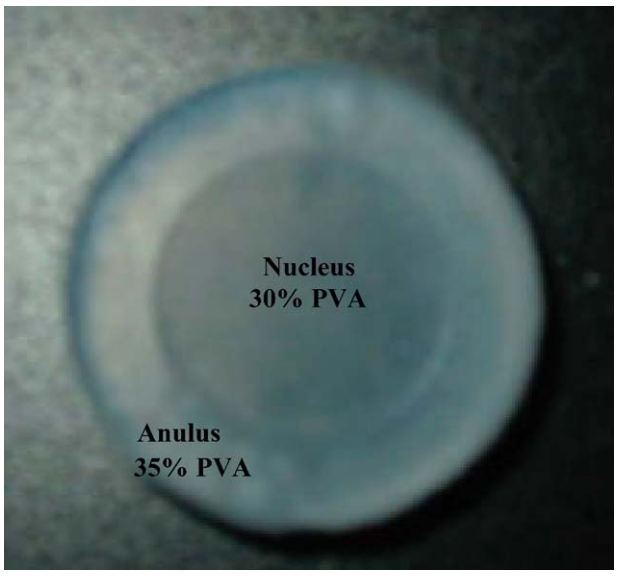

Figure 1 The Intervertebral hydrogel disc model consisting of the inner nucleus (30% PVA) and the outer anulus (35% PVA).

3. Creep experimental test details

A hydrogel disc of known weight was placed in a self contained unit, where it was fully immersed in water and loaded in between porous nylon endplates. The end plates were de-aired by immersing in water and applying a vacuum. In order to maintain full permeability at the hydrogel-endplate interface the hydrogel was left unattached to the endplates by any adhesive. This resulted in some lateral movement at the hydrogel-endplate interface, which had to be accounted for in the subsequent finite element modeling. A screw-driven Instron 4505 mechanical testing machine with a crosshead speed of 10 mm/min was used to ramp the load to 200 N, where it was held for 11 h and 30 min. Both the load (hence stress) and the duration of experiment were chosen to make sure there was a level of fluid loss that was comparable with sustained loading experiments on biological IVD's, without any structural damage to the solid matrix of the hydrogel. The sample was then blot dried and reweighed to determine the fluid loss. By keeping the hydrogel fully immersed in water throughout the course of the experiment it was ensured that any changes in the external environment such as temperature and humidity did not affect the fluid flow characteristics in the hydrogel. The sample was allowed to re-hydrate up to a week before repeat tests were carried out. Four tests were carried out on two samples S1 and S2 within a period of one month.

4. Finite element modelling

An axisymmetric finite element model of the hydrogel disc was developed using the general purpose finite element package, ABAQUS [20] with the primary aim of simulating the experimentally determined fluid loss values for the hydrogel model. To model the fluid/solid interactions in the hydrogel a time dependant coupled pore pressure/effective stress analysis was performed using the CONSOLIDATION parameter and the SOILS option. Under the poroelastic consolidation formulation in ABAQUS, the hydrogel was treated as a porous medium made of a voided solid matrix (skeleton) and an interstitial fluid (pore fluid) that occupied the voids giving a fully saturated medium. The total stress acting on a point in the medium was assumed to consist of a macroscopic averaged pressure stress expressed as the "excess pore pressure", carried by the fluid and an averaged solid stress termed the "effective stress", carried by the solid skeleton.

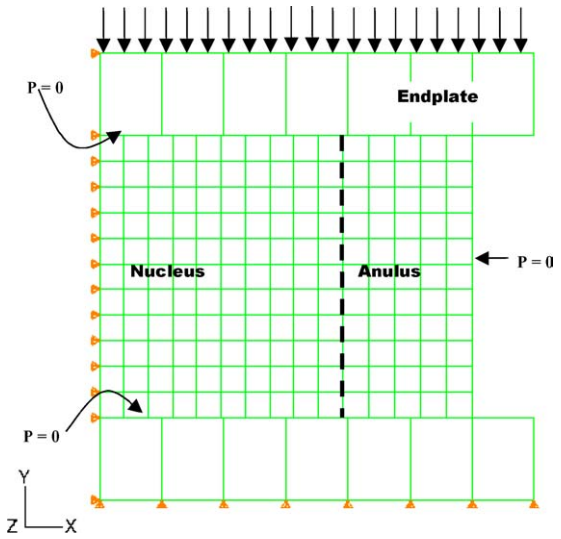

Figure 2 Finite element model of the combined hydrogel disc with applied displacement boundary conditions and pore pressure, $P = 0$ at permeable boundaries.

The finite element mesh consisting of 160 elements representing the nucleus and the anulus was modeled (Fig. 2) using axisymmetric 4 node hybrid solid elements with pore pressure (CAX4PH) for the poroelastic analysis while the end plates were modeled as axisymmetric solid elements (CAX4R). By using solid elements rather than pore pressure elements for the end plates, it was possible to simulate the free draining condition at the hydrogel-end plate interface. Thus, the simplification enabled the introduction of well defined boundary conditions avoiding the greater complexity and uncertaintities in model parameters associated with simulating the contact problem between two poroelastic materials.

The model was created based on the dimensions of sample, S1, where the swollen nucleus and the anulus were 19.01 and 29.14 mm respectively in diameter and 10.40 mm in height. The anulus and the nucleus were treated as homogeneous isotropic materials with strain dependant permeability values. The contact between the endplate and the hydrogel was modeled using the CONTACT PAIR option with finite sliding and a static coefficient of friction to simulate lateral movement at the hydrogel-endplate interface. The NLGEOM parameter was included to account for geometric nonlinearities.

The loading and boundary conditions were matched with that of the experiment. A free draining condition was maintained at the hydrogel surface at all times by specifying a zero pore pressure at the boundary nodes (Fig. 2). The load was applied using a distributed pressure across the top end plate with the bottom end plate left constrained with respect to motion in the loading direction.

5. Material property evaluation

The material input properties for the finite element model were determined by carrying out compression studies under the arrangement described above, separately for fully swollen PVA discs of 30 and 35% PVA composition loaded in two types of compression tests. The elastic solid skeleton stiffness was evaluated for the 30 and 35% PVA materials by loading the hydrogels at a displacement rate of 3 μm/min to obtain the stress/strain response. At such a slow strain rate, there was sufficient time for the excess pore fluid to be drained enabling the solid skeleton to carry the entire applied load in accordance with the theory of consolidation [21]. The discs were also compressed in a static compression test at 100 N for 4 h to obtain the strain dependant permeability values based on measured fluid loss. Separate finite element models were developed for the single materials to validate the material properties. The 4 h compression test was divided into two phases; the loading stage and the consolidation stage. In the loading stage the load was incremented to the applied maximum at a crosshead speed of 10 mm/min. This stage did not involve any fluid loss (Table I) and the fluid and the solid skeleton combined to give an incompressible behaviour. The axial deformation recorded in this stage was affected by the solid skeletal stiffness of the material E, the voids ratio v and the coefficient of friction μ at the hydrogel endplate interface. A value of $\mu = 0.25$ was predetermined for both the materials for this experimental arrangement [19]. For each material the initial experimental deformation during loading was matched by adjusting the values of E and v in the finite element mode (Fig. 3). The consolidation stage consists of the deformation that takes place following the initial loading response and the consolidation strain is the strain response over this stage. A summary of the systematic evaluation process for the 30 and 35% PVA hydrogels is shown in Fig. 3.

The initial permeability values, k_0, for the two materials were estimated using the modified Carman Kozeny equation [22] (see Appendix A). The strain dependant permeability relationship in Equation 1 [23] was adjusted to match the measured fluid loss values for each material over the consolidation stage of the experiment.

$$\kappa = \kappa_0 \left[\frac{e(1+e_0)}{e_0(1+e)}\right]^2 \exp\left[M\left(\frac{1+e}{1+e_0} - 1\right)\right] \quad (1)$$

where e, the voids ratio, is the ratio of fluid to solid for a saturated gel and M is an experimental constant. The subscript 0 indicates the undeformed values. A value of $M = 12$ was used for both the nucleus and the anulus to match the experimental fluid loss. The initial voids ratio e_0 was estimated for each of the materials separately using Equation 2,

$$e_0 = V_f / V_S = (m_f * \rho_f)/(V_T - V_f) \quad (2)$$

TABLE I The experimental and finite element fluid loss values for 30 and 35% PVA compositions at a creep load of 0.1 kN for 4 h

	30% PVA ($n = 2$)		35% PVA ($n = 2$)	
Sample	1 min	4 h	1 min	4 h
Experimental	0	5.58 (6.16)%	0	3.78 (4.16)%
FEA	0	6.33%	0	4.45 %

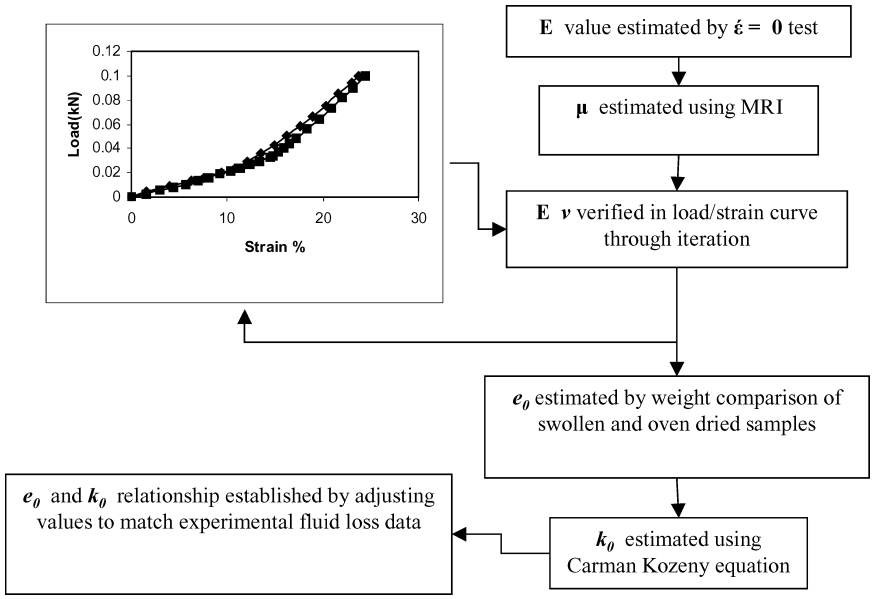

Figure 3 The systematic evaluation of material properties for 30 and 35% PVA hydrogel discs.

where m_f is the mass of fluid determined by oven drying a fully swollen hydrogel sample of volume V_T (where $V_T = V_S + V_f$) at 45 °C for 72 h. V_f and V_S are the volumes of fluid and solid components respectively and ρ_f is the density of fluid, water in this case. The material properties established for the 30 and 35% PVA compositions (Table II) were then used in the combined disc simulations.

6. Results and discussion

The dimensions of the discs used for material testing the 2 compositions were identical and hence the stress dependant axial strain can be used as a measure of the difference in stiffness response between the two materials. Strain values at the end of the loading phase for the 2 PVA compositions over the loading phase (Figs 4(a) and (b)) indicate that both materials had stiffness values that were very close to each other. The strain in the consolidation phase (Figs 4(b) and (d)) clearly indicates that the 30% material experiences a higher axial strain. The higher fluid loss value for the 30% PVA hydrogel (Table I) indicate a higher permeability when compared to the 35% PVA. This is expected owing to the larger pore sizes from a less denser solid matrix in the 30% PVA. The results from the 3 μm/min test indicated that the 35% PVA had a higher stiffness value than the 30% PVA as the strain increased above 30%. However in the lower regions the differences were negligible. Hence a value of 0.45 MPa was used for both compositions as the combination of E, μ and ν (Table II), gave a good match for both PVA compositions over the loading phase.

TABLE II The material parameters used for the 30% PVA nucleus and the 35% PVA anulus

	E (MPa)	e_0	ν	k_0 (mm/s)	M
Nucleus (30% PVA)	0.45	3.0	0.2	0.00025	12
Anulus (35% PVA)	0.45	2.4	0.2	0.00025	12
End Plate	10000	–	0.3	–	–

Although the same initial permeability was used for both materials, their dependency on the voids ratio according to Equation 1, meant that the overall fluid flow was different for the two materials. The parameter M in Equation 1 controls the rate of change of permeability, k with voids ratio, e. The same value of $M = 12$ was arrived at for both materials independently of each other to match the experimental fluid loss values. The specimen rapidly absorbs water following the release of the load, a phenomenon observed in articular cartilage following similar consolidation testing [24]. Therefore the experimentally measured fluid loss values by blot dry method were estimated to be within a 10% error margin. The experimental values were modified to account for an extra 10% of the measured value (indicated within parenthesis Table I), and the permeability values in the finite element model adjusted to match the modified experimental values. The finite element predicted fluid loss (calculated from the sum of volume loss over each finite element) for the 30% (error 2.27%) and 35% PVA (error 6.97%) indicated a good agreement between experiment and simulation and justified the use of the strain dependant permeability values for the combined hydrogel IVD model. Despite the good accuracy between the experimental and the finite element fluid loss values, the experimental strain plots (Figs 4(b) and (d)), indicated that the hydrogels underwent a higher deformation than predicted by a pure consolidation finite element model, with isotropic permeability. The additional deformation is believed to be due to the viscoelastic nature that is common in these polymeric materials. However this viscoelastic behaviour does not appear to contribute to any fluid loss. This is because, immediately following the loading stage (approx. 30 s), the material itself continues to deform even though fluid loss occurs after the 1 minute mark (Table I).

The creep test results (Table III) for the two combined hydrogel discs S1 and S2 show consistency with respect

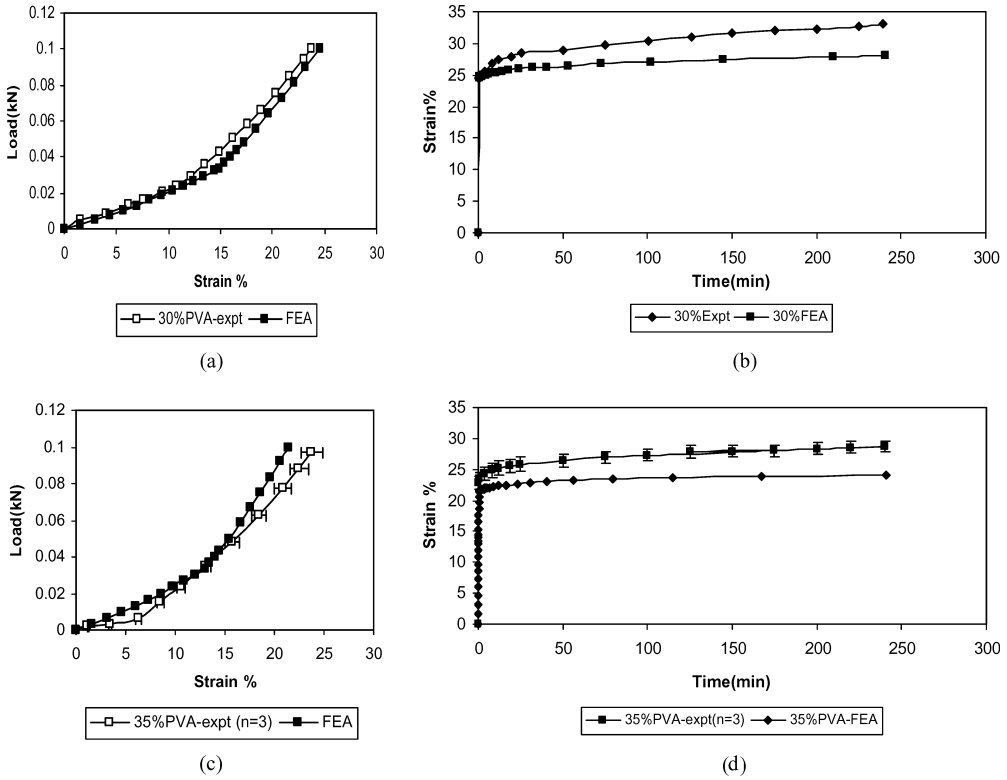

Figure 4 (a) 30% PVA loading response, (b) 30% PVA creep strain, (c) 35% PVA loading response, (d) 35% PVA creep strain (Load increased to 0.1 kN and held for 4 h while the specimen was allowed to consolidate).

to fluid loss and weight recovery. The level of recovery following compression loading serves as a good indicator of the integrity of the solid matrix and whether or not damage to the matrix has occurred. If damage occurs upon loading, which is most likely caused by the breaking of the weak physical hydrogen bonds in the hydrocarbon chain [6], the specimen is seen to increase in weight to that prior to loading within a period of 2–3 days. Values for both samples (Table III) suggest a level of recovery between 92–98% of the original weight (total of 6 specimens), following a recovery time of up to 2 weeks, which further indicates that matrix disruption is minimal. Hence the permeability can be expected to remain unchanged giving rise to a similar quantity of fluid flow under the same loading conditions. The good repeatability in terms of fluid loss for S1 ($n = 4$, 0.63 ± 0.02) and S2 ($n = 4$, 0.51 ± 0.01) confirms that this to be so. Nonetheless repeated loading results in certain changes to the disc dimensions, believed to be due to the visco-plastic nature of these materials from changes occurring at the molecular chain level, that results in the discs, generally losing height and increasing in diameter (Table III).

TABLE III The fluid loss and consolidation test results for specimens S1 and S2, under 0.2 kN load for 11 h 30 min. D_d—Overall disc diameter, D_n—nucleus diameter, H—Height of specimen

Sample	Starting weight (g)	Weight loss (g)	Consolidation strain (%)	Dimensions (mm) (D_d, D_n, H)
S1-test1	7.64	0.63	10.5	29.14, 19.01, 10.40
S1-test2	7.63	0.66	10.7	28.85, 19.35, 10.25
S1-test3	7.56	0.64	9.9	29.27, 18.86, 10.19
S1-test4	7.51	0.60	9.8	29.34, 19.08, 10.22
S2-test1	7.16	0.51	7.3	28.46, 18.78, 10.33
S2-test2	7.15	0.50	7.4	28.56, 18.73, 10.25
S2-test3	7.13	0.51	7.5	28.49, 18.64, 10.24
S2-test4	7.10	0.50	8.1	28.37, N/A, 10.20

It is reasonable to expect a direct proportionality between the fluid loss and the consolidation strain. However such a trend doesn't clearly emerge (Table III) possibly due to the change in dimension of the specimen (hence the change in the strain calculations). Upon repeated loading there is a tendency for the specimens to become stiffer in their initial response to loading, giving rise to a higher standard deviation in the loading phase strain ($n = 4$, ± 2.3) (Fig. 5(a)) when compared to the consolidation strain ($n = 4$, ± 0.45) (Fig. 5(b)). The finite element predicted strain over the initial loading phase shows a very good accuracy (98.5% match with loading strain for test1 of S1) (Fig. 5(a)) indicating the validity of material properties chosen through systematic verification for the two separate hydrogel compositions. The finite element predicted fluid loss of 0.756 g (equivalent to 10.90% volume loss) based upon the initial dimensions of S1 (Table III) compares well with the adjusted fluid loss value of 0.693 g (equivalent to 10% volume loss). The discrepancy between adjusted experimental and simulation can be improved by better quality of manufacturing, whereby dimensions of the nucleus and anulus will be more uniform throughout the height of the specimen. Another factor that needs proper investigation is the permeability changes at the nucleus-anulus interface. It is likely that the nucleus may be more restricted in its fluid expression in the combined gel disc when compared to a single component, which would result in a decrease in permeability and an overall decrease in the fluid loss, which

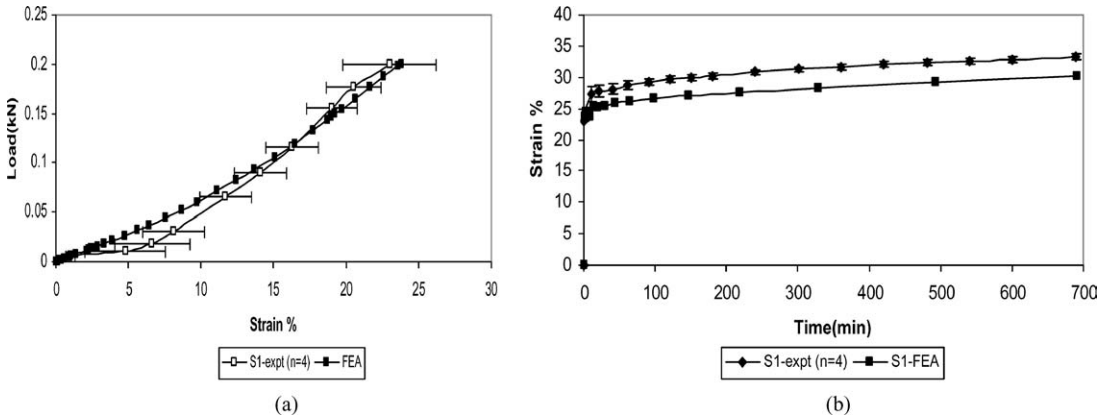

Figure 5 (a) Loading response of combined hydrogel disc -S1 ($n = 4$). (b) Creep strain (Load increased to 0.2 kN and held for 11 h 30 min while the specimen was allowed to consolidate).

the finite element model is not able to capture. The ABAQUS consolidation model predicts water loss according to Darcy's equation [20] where the fluid flow is proportional to the product of the permeability and the applied pressure gradient. Given that there is good agreement between the finite element predicted and the experimental values, the combination of permeability, its variation with strain, the elastic modulus and the voids ratios used in these models are reasonably accurate. Hence, the overall stress pattern predicted by the finite element model is a reasonably good indicator of the actual stress pattern experienced across the hydrogel.

The overall variation in the stress distribution pattern across the hydrogel model shows marked similarities to what is reported for both experimental [25, 26] and finite element [23] cases of stress distribution pattern in biological IVD's under creep loading. The current model demonstrates the important role of the nucleus in load carriage given that the central nucleus initially carries a total compressive load higher than the applied average of 0.35 MPa, also observed for biological IVD's [27]. The differential fluid loss indicating a higher loss from the nucleus (volume loss—13.25%, 0.391 g) over the anulus (volume loss—9.1%, 0.365 g) is accompanied by a fall in the pore pressure over the nucleus (Fig. 6) causing the overall compressive stress to redistribute itself over the entire disc area. This is seen by the increase in the annular solid stress (particularly over

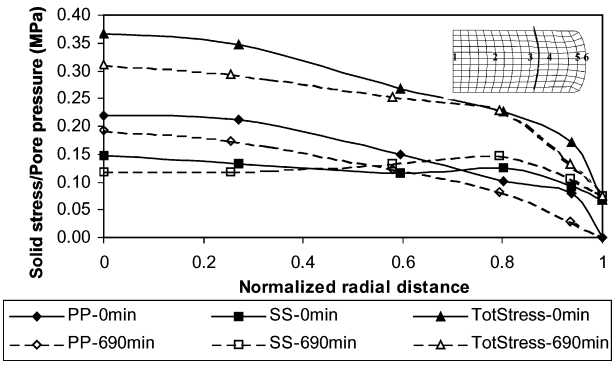

Figure 6 The effect of long term loading on the compressive stress distribution on the hydrogel IVD in the mid radial direction. Regions as marked Nucleus (1–3), Anulus (4–6).

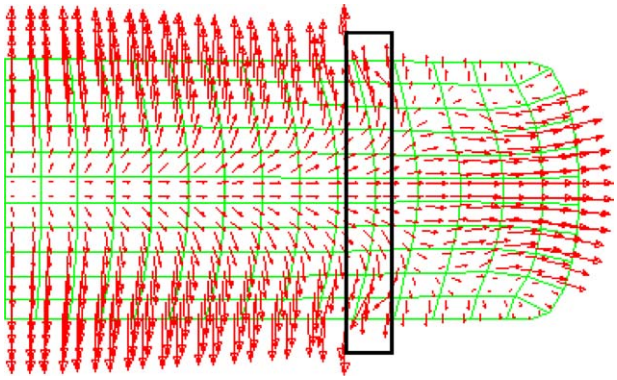

Figure 7 The velocity plot for the hydrogel IVD at 690 min. The area enclosed shows fluid flowing from nucleus to anulus at the nucleus-anulus interface.

point 4) (Fig. 6). The velocity plot for the model (Fig. 7) shows that while the axial pathway through the nucleus is the preferred pathway due to the higher permeability, fluid flows from the nucleus to the anulus, which would indicate a delay in the transference of stress over to the solid component in the anulus. Given that in the biological IVD the radial permeability drops to almost zero in the outermost lamellae thus effectively acting as an impermeable membrane [28] (unlike the current model, which shows fluid loss through the anulus boundary), this radial fluid flow from nucleus to the anulus is possibly a mechanism in the biological IVD to minimise damaging stresses developing in the annular fibres under long term loading, by allowing the fluid to carry the applied load.

7. Conclusion and future work

The intervertebral disc model developed shows important similarities to the natural IVD under compression that includes differential fluid loss, preferential fluid flow and stress transference from nucleus to anulus under long-term creep loading. The model shows a good repeatability with respect to deformation and fluid loss and has potential to be used in future studies that are aimed at understanding better the relationship between fluid flow and applied compressive stress in biological IVD's, using non invasive techniques such as MRI.

The ABAQUS consolidation model implemented is adequate to predict the fluid loss but is unable to capture material creep that is not related to fluid loss. A future improved model would consider incorporating the effects of material creep.

Appendix A

The modified Carman Kozeny equation is given as

$$D = (1 - \rho)d^2/80 \qquad [22]$$

Where D is the permeability of the solid matrix (units m^2), d is the pore diameter (m) and ρ is the relative density of the drained network.

The absolute permeability k (units $m^4N^{-1}s^{-1}$) from Darcy's law and D the permeability are related by $k = \frac{D}{n_L}$ where n_L is the viscosity of the fluid (units $N{\cdot}s{\cdot}m^{-2}$)

Taking the pore diameter for the gel can be considered to be 0.5 μm based on scanning electron micrographs and n_L for water = 0.000891 $N.s.m^{-2}$ and $\rho = 0.9$ which is a reasonable assumption,

$$D = \frac{0.1 \times (5 \times 10^{-7})^2}{80} m^2 = 3.125 \times 10^{-14} m^2$$

from

$$k = \frac{D}{n_L}, \quad k = \frac{3.125 \times 10^{-14}}{0.000891} m^4N^{-1}s^{-1}$$
$$= 3.507 \times 10^{-11} m^4N^{-1}s^{-1}$$

Taking γ_w the specific weight of water to be 9965 $N{\cdot}m^{-3}$ the specific permeability k_s as required by ABAQUS is then found

$$k_s(m/s) = \gamma_w(N \cdot m^{-3}) \times k(m^4N^{-1}s^{-1}) = k_s(m/s)$$
$$= 3.5 \times 10^{-7} m \cdot s^{-1} = 3.5 \times 10^{-4}\ mm \cdot s^{-1}$$

Hence the permeability value that is input as an initial value for the ABAQUS model is in the order of 0.0003 mm/s

Acknowldgements

The present work was partly supported by an Australian Research Council grant. (Grant No. DP0211324) The authors would also like to thank the High Performance Computing Centre in the Queensland University of Technology, Dr Simon Drew of the Centre for Magnetic Resonance for his technical assistance and Ms. Vanessa Ding of the school of Chemical Engineering at the University of Queensland for assisting with the mechanical testing of the hydrogels.

References

1. D. S. McNALLY and R. G. C. ARRIDGE, *J. Biomech.* **28** (1995) 53.
2. N. BOGDUK, "Clinical anatomy of the Lumbar Spine and Sacrum" (United Kingdom, Churchill Livingstone, 1997).
3. E. J. CHIU, in Proceedings of the 43rd Annual Meeting, Orthopaedic Research Society (San Fransisco, CA, 1997).
4. A. E. BAER, M. W. GRINSTAFF, K. A. SMEDS, L. M. BOYD and L. A. SETTON, in Proceedings of the Bioengineering Conference, ASME, 2001.
5. A. S. HOFFMAN, *Adv. Drug Delivery Rev.* **43** (2002).
6. A. S. HOFFMAN, *Ann NY Acad Sci.* **944** (2001) 62.
7. O. WICHTERLE and D. LIM, *Nature* **185** (1960) 117.
8. D. DARWIS, P. STASICA, M. T. RAZZAK and J. M. ROSIAK, *Rad. Phys. Chem.* **63** (2002) 539.
9. L. AMBROSIO, P. A. NETTI, S. IANNACE, J. HUANG and L. NICOLAIS, *J. Mater. Sci.: Mater Med.* **7** (1996) 251.
10. Q. B. BAO and P. A. HIGHAM, US Patent 5,192,326 (1993).
11. M. CIACH and J. AWREJCEWICZ, in Proceedings of the European Medical and Biological Engineering Conference, Vienna, 1999.
12. N. D. BROOM and A. OLOYEDE, *Biomaterials* **19** (1998) 1179.
13. A. A. J. GOLDSMITH, A. HAYES and S. E. CLIFT, ABAQUS Users' Conference, Paris, France, 1995, p. 305.
14. E. WOLFGANG, A. AYHAN and M. BERND, *Proc. Appl. Math. Mech.* **2** (2003).
15. F. YOSHII, K. MAKUUCHI and D. DARWIS, *et al.*, *Rad. Phys. Chem.* **46** (1995) 169.
16. M. KOBAYASHI, J. TOGUCHIDA and M. OKA, *Biomaterials* **24** (2003) 639.
17. J. A. STAMMEN, S. WILLIAMS, D. N. KU and R. E. GULDBERG, *ibid.* **22** (2001) 799.
18. S.-H. HYON and Y. IKADA, US patent No, 4,663,358 (1986).
19. P. SILVA, S. C. DREW, S. CROZIER, M. VEIDT and M. J PEARCY, in Proceedings of the World Congress on Medical Physics and Biomedical Engineering, Sydney [CD-ROM] ISBN 1877040142 paper no. 3677, 2003, p. 4.
20. HIBBIT, KARLSSON and SORENSEN, ABAQUS Theory and User's Manual, version 6.3 (2002).
21. M. A. BIOT, *J. Appl. Phys.* **12** (1941) 155.
22. W. G. SCHERER and R. M. SWIATEK, *J. Non-Cryst. Solids* **113** (1989) 119.
23. M. ARGOUBI and A. SHIRAZI-ADL, *J. Biomech.* **29** (1996) 1331.
24. N. D. BROOM and R. FLACHMANN, *J. Anatomy* **202** (2003) 495.
25. D. S. MCNALLY and M. A. ADAMS, *Spine* **17** (1992) 66.
26. J. CASSIDY, A. HILTNER and E. BAER, *J. Mater. Sci.: Mater. Med.* **1** (1990) 69.
27. A. L. NACHEMSON, *Acta Orthop. Scand.* **S43** (1960) 12.
28. W. Y. GU, X. G. MAO and R. J. FOSTER, *et al.*, *Spine* **24** (1999) 2449.

Received 4 February 2004
and accepted 17 November 2004